RESEARCH ARTICLE
doi: 10.2306/scienceasia1513-1874.2025.s025

ScienceAsia 51S (2): 2025: ID 2025s025: **1–7**

Monotonic manipulation of atomic density in an isovolumetric focused-beam trap for quantum atom experiments

Nuttanan Tanasanchai[a,c], **Kritsana Srakeaw**[a], **Parinya Udommai**[a,b,*], **Waranont Anukool**[a]

[a] Department of Physics and Materials Science, Faculty of Science, Chiang Mai University, Chiang Mai 50200 Thailand
[b] Office of Research Administration, Chiang Mai University, Chiang Mai 50200 Thailand
[c] Thailand Center of Excellence in Physics, Commission on Higher Education, Bangkok 10400 Thailand

*Corresponding author, e-mail: parinya.udommai@cmu.ac.th

Received 17 Dec 2024, Accepted 5 Nov 2025
Available online 20 Dec 2025

ABSTRACT: We present an asymmetric focused-beam trap (FBT) of cold Rubidium-85 atoms. Unlike the cold atom preparation using the magneto-optical trap, the FBT has its path of cooling beam occupying only one axis. Since the experiments on these cold atoms usually require additional laser beams or other atom interacting sources, the FBT allows more optical and physical accessibility for these experiments. In our experiment, the cooling beams only occupied one axis, and the crossed repumping beams were in the transverse plane to the cooling beams. By varying the intensity of the repump laser, we have shown that the atomic cloud density can be monotonically manipulated from zero to the maximum value limited by the cooling power. With this monotonic control, we then computationally introduced a scheme for the precision loading of 1–6 atoms into the far-off-resonance optical dipole trap (FORT). Using the FBT for precision FORT loading could enable extensions toward the research areas, such as Rydberg atom, quantum simulation, and quantum computing.

KEYWORDS: atomic and molecular physics, Magneto-Optical Trap, laser cooling and trapping, cold atom

INTRODUCTION

A few years after the first Magneto-Optical Trap (MOT) was demonstrated in 1987 [1], several succeeding trap designs were proposed and verified with particular properties departing from the six-beamed MOT. They may be classified by mechanical protocols [2, 3] and magneto-optical conformation [4–6]. Though the MOT is still most widely employed to prepare cold dense atomic cloud from room-temperature vapor, today's diverse applications demand traps with rather specific characteristics.

In this work, the two-beam magneto-optical trap (TBT) [7] was the system of interest, where the transverse momentum exchange arises from the focused cooling beams. This setup had then been modified into the so-called focused-beam trap (FBT), with the future aim for neutral-atom precision loading of the far-off-resonance optical dipole trap (FORT).

Our asymmetric focused-beam trap (FBT) of rubidium-85 atoms comprises two confocal cooling beams in the z-axis and two normal pairs of counter-propagating repump beams on the transverse plane. Unlike the MOT, where the cooling and repump beams together occupy all three axes, the FBT's cooling beams take up only one axis and its repump beams occupy the other two axes. However, only one counter-propagating pair of the repump beams is sufficient, and it can be on the same axis as the cooling beam. By setting the laser beams in this configuration, the FBT allows more convenient optical access for further experiments on these cold atoms. This allows accessibility of one additional laser beam used for the FORT. In addition to the FORT, the Rydberg excitation [8] will require one more beam path with an overlap of D2 transition laser and Rydberg transition laser. Furthermore, in the quantum bit preparation from an atom, the Raman transition [9] experiment will be used to populate atoms in one of the chosen ground states, which means that one more beam path will enter the trapping region. This emphasizes that integration of these systems requires many optical access axes. Hence, we present the FBT where the cooling beams occupy only one axis. Besides the $F = 2$ to $F' = 2$ transition for repumping, the opto-magnetic configuration is similar to that of the standard MOT.

We have characterized the FBT to optimize independent parameters, i.e., the detuning and intensities of trap beams, the magnetic field gradient, and the background pressure, for the highest atom number. After that the relations among the cloud density, number of atoms, and the total intensity of repump beams were studied. The characteristics of the atom cloud with dependence on the number of trapped atoms can be distinguished into four regimes [10]. These are named the temperature limited regime (low number of atoms), the multiple scattering regime, the two-component regime, and the optically dense regime (high number of atoms). The atom cloud produced from this work was within the second and third regimes. The multi-scattering regime is where the fluorescence photons get reabsorbed by the cloud itself, and, as a result, the radiative pressure limits the cloud density. With increasing number of atoms, the cloud enters the two-component regime, where the greater magnitude of photon re-absorption now spills

Table 1 Independent parameters used to study ρ as functions of I_c and I_r.

Control parameter	ρ vs. I_c	ρ vs. I_r
I_c (mW/cm^2)	1.15 – 10.36	4.95, 6.29, 8.64, 9.97
δ_c (MHz)	−12.0	−12.0
I_r (mW/cm^2)	0.33, 0.62, 2.48, 17.69	0.21 – 17.85
δ_r (MHz)	−12.0	−12.0
∇B (G/cm)	16.48	16.48
P (mbar)	6.04×10^{-9}	5.83×10^{-9}

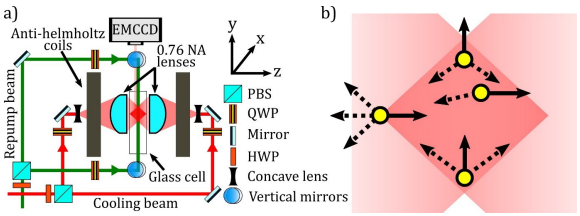

Fig. 1 (a) Schematic of the focused-beam trap. (b) Illustration of atoms entering the trap region from −y and −z. The solid and dashed arrows represent instantaneous atomic velocities and spatially dependent wave vectors, respectively.

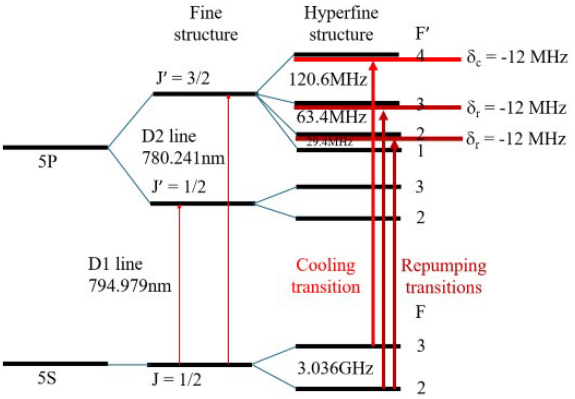

Fig. 2 Energy-level schematic of the Rubidium-85 D2 line [18]. The cooling transition and two repumping transitions are shown, each with −12 MHz red detuning.

atoms out from the harmonic trap into its shallower potential surrounding. As a result, the cloud volume slightly expands and hence lessens the cloud density.

The quantitative analyses of the FBT manifest an unchanged cloud volume over the whole experimental range of atomic density and repump laser intensity. The cloud volume was controlled by varying the trap laser intensity. Within both regimes, we have demonstrated monotonic manipulation of the cloud density by varying only the intensity of the repump beams. The other parameters—namely, the cooling beam intensity, frequency detuning, magnetic field gradient, and vacuum pressure—were kept constant, as later shown in Table 1. Rough estimation of the repumper intensities for loading 1–6 atoms in the FORT is also given to raise the usefulness of our monotonic manipulation of cloud density.

MATERIALS AND METHODS

This work presents the laser cooling and trapping of Rb atoms in the focused beam trap setup whose schematic is shown in Fig. 1a. Fig. 1b illustrates the configuration of two counter-propagating focused laser beams aligned at the glass cell containing Rb vapor. Using the doppler cooling technique [11], the laser frequency was detuned by a few MHz from an atomic cooling transition, i.e., Rb-85: $5S_{1/2}(F=3)\rightarrow5P_{3/2}(F'=4)$, as shown in Fig. 2. Focusing geometry of the beam caused the spatial intensity gradient. As a result, the AC Stark effect [12] was expected to cause the energy level shift in the Rb atoms, which is proportional to the beam intensity. The highest cooling beam intensity used was about 10 mW/cm^2, which corresponded to the AC Stark shift of around −1.4 MHz [13]. This energy shift is significantly low compared to the red-detune of −12.0 MHz (Table 1). It should also be noted that beam focal point, which provided the greatest AC Stark shift, was 5 mm away from the trap center at the inner surface of the glass cell.

Fig. 1b also illustrates forces acting on the atoms subjected to the trapping force from the focused beam configuration. The solid arrows represent instantaneous atomic velocities. The dash arrows represent spatially dependent wave vectors belonging to the cooling beam that was on resonance with the atom. Given that z-axis is along the direction of the cooling beams. Those atoms moving toward the trap center along the z-axis experience the radiation pressure from the cooling beam pointing opposite to the atom motion. This force acting on the atoms are equivalent to the doppler cooling from the optical molasses in the conventional MOT experiment. In addition, since this force is velocity-dependent (i.e., damping force), the atoms are expected to have a damped wavy trajectory near the trap center [14]. Note that the position-dependent force (i.e., restoring force) that brings atoms to the trap center is added to the setup using the magnetic field effect from the anti-Helmholtz coils (shown in Fig. 1a).

Those atoms moving on the xy transverse plane experience a net-zero radiation force along the z-axis. On the xy-plane, due to the focused geometry of the beams, the intensity gradient [13, 15] of the red-detuned beams results in the net force oriented toward the z-axis, regardless of atoms' velocity. However, the doppler cooling is only effective on the outbound course where the velocity is opposite to the net force. The trap loss is inevitably dominated by those atoms moving toward the z-axis and accelerated by the net force. This loss mechanism is reflected in the higher temperature of the trapped atoms along the xy-plane

compared to that along the z-axis. All in all, the FBT could still provide three-dimensional cooling and confinement owing to the transverse momentum exchanges through atom-light scattering process.

In this work, all self-made external cavity diode lasers employed the cateye configuration [16]. For the cooling beams, the linearly polarized laser (diode: DL-780-90) was divided by a polarization beam splitter (PBS) into 68 mW and 2 mW of power. The weaker beam was sent to the single-beamed Doppler-free saturated absorption spectroscopy (DSAS) [17]. The higher power beam was locked at 5.0 MHz below the $5S_{1/2}$(F=3)→$5P_{3/2}$(F′=3,4) crossover transition by using the feedback signal from the DSAS produced using the weaker beam. The cooling beam was injected into a double-pass 80 MHz acousto-optic modulator (AOM). It was then amplified at a tapered chip (EYP-TPA-0780-01000-3006-CMT03-0000) before doubly passing through a 110 MHz AOM. This section permits both varying the intensity and shifting the frequency within a range of 20–100 MHz from the atomic transition, as mentioned.

Single-mode optical fibers were used as laser waveguides that separated the beam preparation from the experimental space around the rectangular rubidium cell (1.00 cm × 2.00 cm × 9.75 cm of inside dimensions). Right after the outward-bound fiber coupler, the cooling laser was equally split using the PBS. Each split beam was set to σ^+ circular polarization and another to σ^- circular polarization. On both sides of the rubidium cell, a 32 mm focal-length concave lens and a 0.76 NA lens (ACL50832U-B) were combined to tightly focus each cooling beam. Two focused cooling beams were then counter-propagating and overlapped one another in the glass cell, as shown in Fig. 1. This is a confocal arrangement along the z-axis at Fourier plane separation of 1.00 cm.

During the experiment, the repump laser (diode: L785P100) was kept locked using similar DSAS configuration at the frequency detuning of 2.7 MHz above the $5S_{1/2}$(F=2)→$5P_{3/2}$(F′=1,2) crossover in the D2 transition. A pair of half-wave plate (HWP) and PBS helped to attenuate the power of the repump beam before getting expanded from 1.62 mm to 6.82 mm of diameter. These beams provide the overlap volume well covering the whole cooling region. The repump laser was split and circularly polarized in the same manner as the cooling beams. Two normal pairs of counter-propagating repump beams lying on the xy-plane intersect the trap beams at the center of the glass cell, coinciding with the zero magnetic field from the anti-Helmholtz coils.

The experiment began with an optimization of the FBT to find a set of independent parameters close to the maximal efficiency pertaining to the highest atom number (N). The optimal magnetic field gradient ($\boldsymbol{\nabla}B$), background pressure (P), detuning (δ_c), and intensities (I_c) of cooling beams were determined and concluded in Table 1. For additional information, the experimental setup was operated at room temperature conditions, and so was the rubidium cell's temperature.

According to the broad plateau of the cloud density (ρ) vs. $\boldsymbol{\nabla}B$ observed beyond 15.0 G/cm, we only executed experiments at 16.48 G/cm. In order to verify that I_c = 4.95 mW/cm^2 is well within the multi-scattering regime, a series of experiments for ρ versus I_c has been conducted at four fixed values of repump intensities, i.e., I_r = 0.33, 0.62, 2.48, and 17.69 mW/cm^2. With all parameters defined, the physical connections among ρ, N, and I_r can be investigated by varying the repumper intensity from 0.21–17.85 G/cm. Three ρ versus I_r experiments performed at I_c > 4.98 mW/cm^2 are to confirm the consistency of parametrical setup.

To obtain a large damping rate for cooling in the z-axis, we detuned the trap laser by −12.0 MHz from the $5S_{1/2}$(F=3)→$5P_{3/2}$(F′=4) transition, as shown in Fig. 2, which is approximately twice the natural line width. By slowly changing the external cavity length, the frequency scanning has identified two comparable maxima of the florescence signal at the repumper detuning (δ_r) of −75.4 MHz and −12.0 MHz from the $5S_{1/2}$(F=2)→$5P_{3/2}$(F′=3). The −75.4 MHz detuning is equivalent to δ_r = −12.0 MHz from the $5S_{1/2}$(F=2)→$5P_{3/2}$(F′=2) (Fig. 2). Additionally, since this experiment involved two excitation paths with the same $5P_{3/2}$ excited state, one may refer to this as the Raman transition [19]. This was not the case because the excitation by the repumper has different hyperfine upper levels from that of the cooling beam.

The Raman photons from the repump beam mediate population transfer between the two hyperfine ground states, effectively recycling atoms from the dark (F = 2) to the bright (F = 3) state. This process determines the steady-state atom number by balancing atom loss and recovery within the cooling cycle. The Raman scattering rate depends on the repump intensity and its detuning: small red detuning enhances repumping efficiency and increases atom number, while large detuning reduces the scattering rate, allowing atoms to accumulate in the dark state. The chosen δ_r = −12.0 MHz provides an optimal balance between efficient repumping and minimal heating, ensuring stable atom number in the cold cloud. To avoid bias from the bright-state population, we simultaneously detected the cold atoms in both hyperfine ground states (F = 2 and F = 3) using the repump and trap beams, respectively, thereby obtaining the total atom number independent of the bright-dark state distribution.

RESULTS AND DISCUSSION

This section presents the analysis of trapped cold cloud of Rubidium-85. Gaussian fitting routine on a picture of the cold cloud taken using fluorescence imaging technique (EMCCD camera: Andor iXon 897) yielded

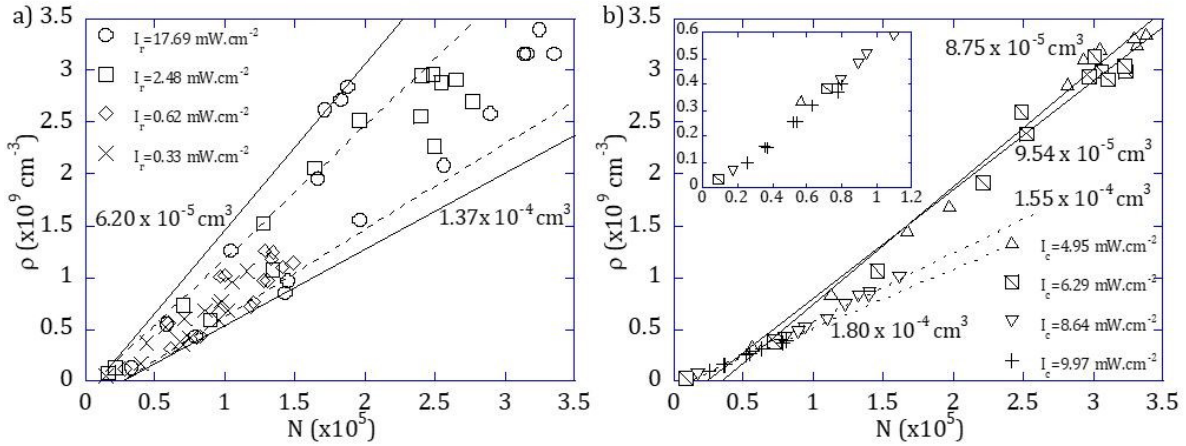

Fig. 3 Cold cloud density (ρ) as a function of the atom number (N) when a) varying the trap beam intensity (I_c) along with four fixed repumper intensity (I_r) and b) varying the I_r along with four fixed I_c. Each fit line in Fig. 3b corresponds to a constant volume at fixed I_c. For clarity, the density error bars are shown only in Fig. 4, as the corresponding errors in Fig. 3 are small for visualization (average SD of 3%). The inset magnifies the plot at low density.

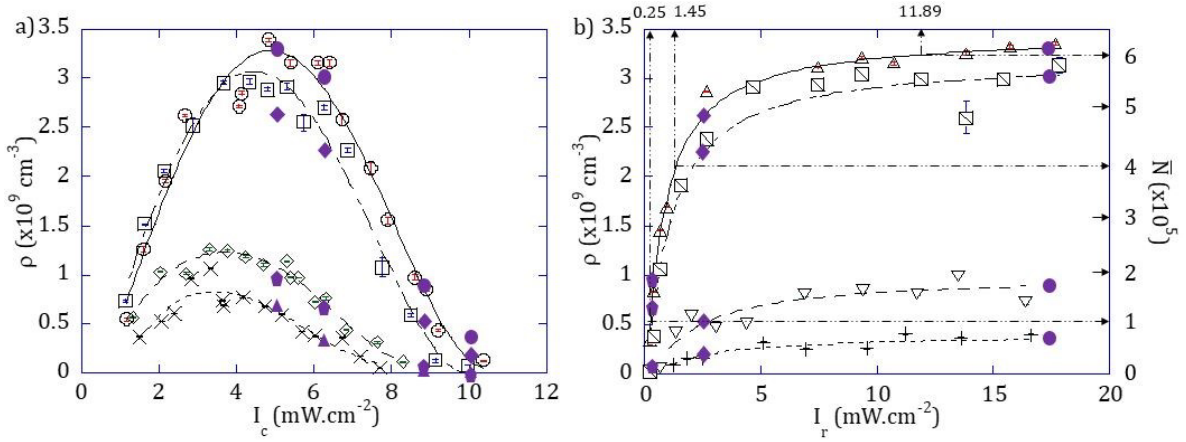

Fig. 4 Dependence of the cloud density (ρ) on the intensities of a) the trap laser (I_c) and b) the repump laser (I_r), using the same symbols as described in Fig. 3. The filled symbols indicate the cloud densities at constant I_r, while a set of four different filled symbols represents a constant cloud volume within the same trap regime. All filled symbols are marked on the fit curves in Fig. 4b and then linked back to Fig. 4a for consistency checking. The polynomial fits are for guidance. The rightmost axis shows the average number of trapped atoms (N_{FORT}) expected in the FORT with a beam waist of 1.2 μm at the center of the FBT. The three repumper intensity values shown at the top are taken from Table 2. Error bars of I_c and I_r are within the size of symbols.

the atom number, while the number of rubidium-85 atoms in steady state was estimated by exponential fit of the loading curve. Since the cloud geometry was best described by an oblate spheroid, the volume of the ensemble was calculated using the radii along two semi-axes that correspond to e^{-1} peak signals. The temperature was estimated employing the free expansion method [20]. The studies on the effects of trap beam and repumper intensities were carried out by increasing and decreasing the fields, respectively, while maintaining the trap geometry, beam sizes, and polarizations. A few data points had been repeated to check for parametric consistency and were included in the analyses. The measured quantities were averaged over ten successive identical experiments. All coherent optoelectronic and magnetic operations were controlled by a self-made timing sequence generator with a resolution of < 100 μs. Unless otherwise stated, physical values in the following discussion are related to $I_c = 4.95$ mW/cm^2 and $I_r = 17.69$ mW/cm^2, which gave the maximum density.

According to the operation principle of the FBT

Table 2 Repump laser intensities estimated for loading 1–6 atoms in the FORT with a beam waist of 1.2 μm. The mean target atom number (N_{FORT}) was evaluated assuming Poissonian statistics over 10 loading shots.

N_{FORT}	N_{FBT} ($\times 10^3$)	ρ_{FBT} ($\times 10^9$ cm^{-3})	I_r (mW/cm^2)
1 ± 0.32	48	0.54	0.25
2 ± 0.45	97	1.08	0.49
3 ± 0.55	146	1.62	0.82
4 ± 0.63	194	2.16	1.45
5 ± 0.71	243	2.70	2.93
6 ± 0.77	292	3.24	11.89
7 ± 0.84	341	3.78	–

illustrated in Fig. 1b, the trap depth is well defined only along the z-axis. By using the scattering force at half maximum and the trap radius $r_z = 5.0$ mm, this FBT setup allowed for the MOT capture velocity of $v_c = \sqrt{hk\Gamma r_z/2m_{Rb}}$, which corresponds to the trap depth of $T_c = hk\Gamma r_z/2k_B = 5.86$ K [14]. k is the laser's wave number, Γ is the natural linewidth of Rb's D2 line, and m_{Rb} is mass of one Rb-85 atom. This trap depth suggests the maximum atom speed or temperature along the z-axis that this FBT setup can still trap. The gaseous spheroids were flattened along the z-axis by approximately 30% of the radius from a perfect sphere. The largest trap volume had semi-axis lengths of 237 μm and 310 μm.

While varying the cooling beam intensity, the loading times, ranging from 387 ms to 634 ms, were almost independent of the repumper intensity. The lowest temperatures measured for the cloud were 41.7 μK on the z-axis and 270.9 μK on the xy-plane. The temperature was estimated using the release-recapture technique, which depends on the atomic cloud radius and here yielded a significantly low SD. The quoted temperatures represent the measured values with associated uncertainties. The higher temperature on the xy-plane was due to focused beam geometry that allowed for trap loss as mentioned in Methodology. The Doppler temperature of 145.6 μK for Rb-85 atoms suggests that polarization gradient cooling was not as effective as in the standard MOT along the symmetry axis and has not been activated on the plane containing minor axes, probably due to the heating effect of the Stokes Raman scattering.

Fluorescence photons from an atomic cloud were collected using two convex lenses with 35 mm and 50 mm focal length placing at 70 mm and 240 mm, respectively, from the trap center. As a result, the atomic cloud image appeared at 340 mm from the trap with 1:1 size ratio. The cloud radius was defined as the $1/e^2$ radius from the Gaussian fit of the cloud image. Since over a hundred frames were taken for each measurement, the standard deviation was used as the uncertainty. The extracted radii were further used for the analysis of cloud volume and atom number density.

The maximum density observed was 3.35×10^9 cm^{-3} at optimal conditions, i.e., $I_c = 4.95$ mW/cm^2, and $I_r = 17.69$ mW/cm^2, and almost constant within 20 μm of radius from the trap center in all directions. With similar intensities of the trap and repumper beams, the conventional 3D MOT has the typical atomic density of a few 10^{10} cm^{-3} [21], which is comparable to the value achieved in our work. At four fixed I_r values (Fig. 3a), the trap beam geometry confined atoms to a volume of $(6.20–13.7)\times10^{-5}$ cm^3, bounded by two solid lines. The behavior of ρ versus I_c (Fig. 4a) shows a non-monotonic relation within the multi-scattering regime, which is of interest in this work.

We varied I_r to further investigate the FBT in the multi-scattering and two-component regimes with different values of $I_c = 4.95–9.97$ mW/cm^2 (Fig. 3b). While the standard MOT demonstrates constant number of atoms up to $N = 10^{10}$ atoms [21], the tight confinement of the FBT seems to impose strong restriction on both density and the atom number to undergo changes with I_c at the same rate as shown in Fig. 3b. The linear relationship of ρ versus N implies constant volume, since the density was calculated from $\rho = N/V$. The number of atoms and the volume were extracted from the atomic cloud images. Therefore, the linear relationship between density and atom number indicates that the volume is constant. In Fig. 3b, four volume measurements of $8.75\pm0.98\times10^{-5}$, $9.46\pm1.50\times10^{-5}$, $1.53\pm0.19\times10^{-4}$, and $1.79\pm0.18\times10^{-4}$ cm^3 were observed at $I_c = 4.95$, 6.29, 8.64, and 9.97 mW/cm^2, respectively. This feature also implies that the cloud volume changes only with I_c and not with I_r. Counting atoms in both hyperfine ground states using the scattering rate of the $F = 3$ to $F' = 4$ transition yielded an underestimated N. However, at a constant volume, the linear relation of ρ versus N remains on the same straight line.

The atomic density of the cold cloud strongly depends on the loading rate and the loss rate. The saturated densities in Fig. 4a are given by the balance between the confining force and the multiple scattering force. The first one is not harmonic since it is the combination of the damping force on the inbound and restoring force on the outbound of propagating atoms. The second is the competition between the repulsion due to reabsorption of fluorescence photon between atoms and the compression intensified via the shadow effect [22]. The FBT has demonstrated the highest density within a narrow window, $3.0 < I_c < 6.0$ mW/cm^2 (Fig. 4a). In Fig. 4a, as I_c increases beyond this narrow window, the damped harmonic well spills out excessive atoms, resulting in a sharp drop of ρ.

However, the trap beam intensity at $I_c = 4.95$ mW/cm^2 well maintained the clouds in the multi-scattering regime for the whole range of I_r imposed. The local maxima incline toward increasing I_c from ρ

$= 0.83\times10^9$ cm^{-3} to 3.29×10^9 cm^{-3}, in accordance with volumes of $(10.40\pm0.25)\times10^{-5}$ cm^3, narrowed down to the middle zone bounded by dash lines in Fig. 3a. In the present case, the repump-to-cooling intensity ratio has been increased to $\geqslant 11$ times the magnitude generally utilized in the standard MOT. The F=2 ground state would be rapidly depleted while the Stokes Raman transition heats atoms. As a result, no further compression on the xy-plane was observed, which is consistent with the directional measured temperatures. In contrast to the ρ-I_c relation in Fig. 4b, the cloud density and hence N increased monotonically with I_r. It never decreased but smoothly approached the asymptotic line corresponding to the density of 3.45×10^9 cm^{-3} at the optimal cooling intensity.

While most physical properties of the FBT resemble typical MOTs, the effect of repump beams on the number of trapped atoms is radically different from the Wieman-Pritchard model used to describe an additional repulsive force arising from multiple reabsorptions of Stokes Raman photons in the optical thickness regime [21]. Considering the standard MOT, the cooling process would become saturated approximately a thousand times slower than the repumper due to the small leakage out of the $F = 3$ to $F' = 4$ cooling cycle. This implies that weak repump beams are all the Doppler cooling needs, and changing the repumper intensity should not cause a significant effect on the atomic cloud density. In contrast to the FBT geometry, the repumper plays the role of a diligent trap enhancer that could also completely suppress the atom number even at the most efficient cooling intensity. In this work, where the maximum atom number was just 3.35×10^5, by further detuning the repump frequency at -75.4 MHz from the $F' = 3$ hyperfine state, the excited states of the two lasers are well separated, and the I_r-dependence of the cloud density was amplified. Evidently, the increased compression of the cold cloud with growing I_r cannot be understood by integrating the repumper heating of $h(\Delta\omega 23 - 2\pi \times 12.0$ MHz) per Stokes photon scattering as an additional repulsion force in the rate equation. Though including all parameters that influence the capture velocity is too complex, the strong I_r-dependence of the cloud density is expected to behave like $\rho = \rho_\infty(I_r/(I_N + I_r))^2$, directly obtained from a simple rate equation [14]. Here, ρ_∞ represents the maximum density, and I_N represents the intensity at which ground-state repumping rate equals the trap loss rate, or I_N denotes the reference intensity related to the proportion of the hyperfine ground-state populations inside the FBT. We found that the repulsive force due to Stokes photon heating does not overrule the effect of hyperfine ground state conversion to $F = 3$; as a result, the density increased with I_r. We deduced $I_N = 0.38$, 0.49, 1.01, and 1.12 mW/cm^2 in descending order of I_c in Fig. 4b.

To serve the purpose intended for future applications, loading of the FORT from the FBT could be straightforward when both traps share the same pair of high-NA lenses. Since the minimum waist of the FORT is confined to the diffraction limit of the wavelength used, only a tiny overlap volume of the two traps at the cloud center defines the number of atoms that take part. By using the FBT region with nearly constant density and the FORT with beam waist of 1.2 μm, the overlap volume will have the trap geometry prescribed by 40.0 μm and 2.4 μm along the axial and radial axes, respectively. Table 2 shows an estimated calculation of the number of atoms in the FORT with relationship to the number of atoms and also the atom density in the FBT. With the assumption of the Poissonian statistics, average numbers of 1–6 atoms could be transferred into the FORT by varying I_r from 0.25–11.89 mW/cm^2, whereas loading 7 atoms into the FORT would require $I_r > 20$ mW/cm^2, according to the results in Fig. 4b. Selectively trapping more than two atoms in the FORT is beyond the practical limit of the blue-detuned, light-assisted loading [23, 24]. To use the scheme illustrated in Fig. 4b, the values of I_r must be evaluated for distinct trap conformation. Stabilizing I_r would put the loading close to the most probable atom number when the Poissonian statistics are assumed. In addition, an atom counting technique will be required to verify the loading variation from shot to shot. However, this shows only an estimate under ideal Poissonian statistics; in practice, several parameters could affect the capability of loading one or more atoms into the FORT. These parameters include, for example, the laser stability, which causes atomic cloud fluctuation, and the FORT laser beam stability, which affects the trap depth.

As a result, deterministic preparation and defect-free single atom traps are achievable. This can enable the next generation of single-atom experiments, such as atom rearrangement, Raman transition experiment, and Rydberg atom experiment. The fields that this can advance include quantum simulation of complex many-body systems [25, 26], which demand selectable degrees of freedom at prescribed lattice defects. Among other applications, the quantum simulation of complex chemical systems and the development of new materials could be pursued based on these trapped atoms. In addition, quantum information processing that utilizes the FORT atoms as quantum bits has been an active area of research, paving the way toward a quantum computer [27, 28].

CONCLUSION

Preparation of the atomic cloud of cold Rubidium-85 was demonstrated in the focused-beam trap experiment. This was to enable an alternative method to the conventional three-dimensional magneto-optical trap. The FBT configuration allowed more convenient optical access for extensions of experiments from this

atomic cloud, such as the far-off-resonance trap and Rydberg excitation. Our FBT demonstrated the atomic cloud volume was not influenced by varying the repumper intensity I_r up to 17.85 mW/cm^2 and the cloud density up to 3.35×10^9 cm^{-3}. Without varying the cooling beam intensity I_c, the spontaneous Raman photons from an intensified repump laser permitted monotonic manipulation of the number of atoms from zero to the maximum number limited by the cooling power. Our FBT arrangement could provide an alternative precision loading of the far-off-resonance trap, depending on influential experimental parameters, such as the stability of the lasers.

Acknowledgements: The authors would like to express their gratitude to Prof. Emeritus Dr. Thiraphat Vilaithong and Prof. Dr. Sitthichai Pokai-udom. Deep appreciation is given to National Astronomical Research Institute of Thailand, Mahanakorn University of Technology and Synchrotron Light Research Institute. This work was supported by CMU Junior Research Fellowship Program, National Research Council of Thailand and Fundamental Fund 2568.

REFERENCES

1. Raab EL, Prentiss M, Cable A, Chu S, Pritchard DE (1987) Trapping of neutral sodium atoms with radiation pressure. *Phys Rev Lett* **59**, 2631–2634.
2. Monroe C, Swann W, Robinson H, Wieman C (1990) Very cold trapped atoms in a vapor cell. *Phys Rev Lett* **65**, 1571–1575.
3. Harvey M, Murray AJ (2008) Cold atom trap with zero residual magnetic field: the ac magneto-optical trap. *Phys Rev Lett* **101**, 173201.
4. Liebisch TC, Blanshan E, Donley EA, Kitching J (2012) Atom-number amplification in a magneto-optical trap via stimulated light forces. *Phys Rev A* **85**, 013407.
5. Lee KI, Kim JA, Noh HR, Jhe W (1996) Single-beam atom trap in a pyramidal and conical hollow mirror. *Opt Lett* **21**, 1177–1179.
6. Stites R, McClimans M, Bali S (2005) Large atom-density change at constant temperature by varying trap anisotropy in a dilute magneto-optical trap. *Opt Commun* **248**, 173–178.
7. Chesman C, Lima EG, Oliveira FAM, Vianna SS, Tabosa JWR (1994) Two- and four-beam magneto-optical trapping of neutral atoms. *Opt Lett* **19**, 1237–1239.
8. Zuo Z, Fukusen M, Tamaki Y, Watanabe T, Nakagawa Y, Nakagawa K (2009) Single atom Rydberg excitation in a small dipole trap. *Opt Express* **17**, 22898–22905.
9. Wineland DJ, Monroe C, Itano WM, Leibfried D, King BE, Meekhof DM (1998) Experimental issues in coherent quantum-state manipulation of trapped atomic ions. *J Res Natl Inst Stand Technol* **103**, 259–328.
10. Palittapongarnpim P (2012) Characterization of magneto-optical trap for experiments in light atom interfacing. MSc thesis, University of Calgary, Canada.
11. Phillips WD (1998) Laser cooling and trapping of neutral atoms. *Rev Mod Phys* **70**, 721.
12. Black JA, Schmidt H (2014) Atomic cooling via AC Stark shift. *Opt Lett* **39**, 536–539.
13. Grimm R, Weidemüller M, Ovchinnikov YB (2000) Optical dipole traps for neutral atoms. *Adv At Mol Opt Phys* **42**, 95–170.
14. Metcalf HJ, van der Straten P (1999) *Laser Cooling and Trapping*, Springer, New York, USA.
15. Neuman KC, Block SM (2004) Optical trapping. *Rev Sci Instrum* **75**, 2787–2809.
16. Thomson DJ, Scholten RE (2012) Narrow linewidth tunable external cavity diode laser using wide bandwidth filter. *Rev Sci Instrum* **83**, 023107.
17. Svanberg S, Yan GY, Duffey TP, Schawlow AL (1986) High-contrast Doppler-free transmission spectroscopy. *Opt Lett* **11**, 138–140.
18. Steck AD (2010) Rubidium 85 D Line Data. University of Oregon, USA.
19. Prince RC, Frontiera RR, Polma EO (2017) Stimulated Raman scattering: from bulk to nano. *Chem Rev* **117**, 5070–5094.
20. Arora P, Chowdhury S, Agarwal A, Pant K, Gupta AS (2011) Characterization of cold atomic cloud in a magneto-optical trap. *Indian J Pure Appl Phys* **49**, 590–595.
21. Gattobigio GL, Pohl T, Labeyrie G, Kaiser R (2010) Scaling laws for large magneto-optical traps. *Phys Scr* **81**, 025301.
22. Dubetsky B, Berman PR (1997) *Atom Interferometry*, Academic, Chestnut Hill.
23. Grunzweig T, Hilliard A, McGovern M, Andersen MF (2010) Near-deterministic preparation of a single atom in an optical microtrap. *Nat Phys* **6**, 951–954.
24. Sompet P, Carpentier AV, Fung YH, McGovern M, Andersen MF (2013) Dynamics of two atoms undergoing light-assisted collisions in an optical microtrap. *Phys Rev A* **88**, 051401.
25. Lahaye T, Barredo D (2022) Quantum simulation and computing with arrays of single Rydberg atoms. *Europhys News* **53**, 28–31.
26. Brantut JP, Donner T (2022) Quantum simulation with atoms and photons. *SPG Mitt* **67**, 25–29.
27. Evered SJ, Bluvstein D, Kalinowski M, Ebadi S, Manovitz T, Zhou H, Li SH, Geim AA, et al (2023) High-fidelity parallel entangling gates on a neutral-atom quantum computer. *Nature* **622**, 268–272.
28. Bluvstein D, Evered SJ, Geim AA, Li SH, Zhou H, Manovitz T, Ebadi S, Cain M, et al (2024) Logical quantum processor based on reconfigurable atom arrays. *Nature* **626**, 58–65.